Microfluid Nanofluid (2017) 21:142
DOI 10.1007/s10404-017-1975-7

RESEARCH PAPER

From flow focusing to vortex formation in crossing microchannels

Iulia Rodica Damian[1] · Steffen Hardt[2] · Corneliu Balan[1]

Received: 22 May 2017 / Accepted: 21 July 2017 / Published online: 10 August 2017

Abstract The paper is concerned with the experimental and numerical investigations of the vortex formation and flow focusing inside a cross-shaped microchannel domain. The local hydrodynamics in the junction area, upstream of the focusing region, is analyzed with the aim to characterize the onset and the evolution of the vortical structures, in correlation with the operating parameters. The numerical simulations based on a finite-volume approach are validated by direct flow visualizations using epifluorescence and confocal microscopy. The main result of the study is a flow pattern map, providing comprehensive information on the flow dynamics inside the microchannel junction as a function of the input flow rates and the corresponding Reynolds numbers. The flow pattern map identifies the limits of the flow focusing regime and the critical values of the parameters at which the vortical structures are formed. Beyond the breakdown of the classical flow focusing scenario with one focused output stream, flow patterns with two and four output streams are identified.

✉ Steffen Hardt
hardt@nmf.tu-darmstadt.de

Iulia Rodica Damian
rodica.damian@upb.ro

Corneliu Balan
corneliu.balan.@upb.ro

1 Hydraulics Department, REOROM Laboratory, Politehnica University of Bucharest, Splaiul Independentei 313, 060042 Bucharest, Romania

2 Institute for Nano- and Microfluidics, TU Darmstadt, Alarich-Weiss-Straße10, 64287 Darmstadt, Germany

Keywords Microchannel · Cross-junction · Vortex formation · Flow focusing · Fluorescence microscopy · CFD

1 Introduction

Focusing fluids and mixing in microchannel systems are among the most common applications in microfluidics. The hydrodynamics in micro-junctions involves complex flow patterns, even though the Reynolds numbers are normally small enough to keep the flows in laminar regime. The present study is dedicated to the experimental and numerical investigation of the flow dynamics in a cross-micro-junction, close to the onset of flow focusing. In particular, our interest is to determine and to model the vortex formation at the contact of three liquid streams in a micro-junction located upstream of a microchannel, where the focusing eventually takes place.

The hydrodynamic focusing phenomenon has direct applications in the separation, counting or sorting of particles (Rodriguez-Trujillo et al. 2006; Rondeau and Cooper-White 2008; Xuan et al. 2010), assembly of polymers and liposomes (Schabas et al. 2008; Hong et al. 2010; Jahn et al. 2007, 2013) and droplets (Wang et al. 2007; Maenaka et al. 2008; Fu et al. 2012).

The hydrodynamic focusing phenomenon was first used by Spielman and Goren (1968) for particle counting analysis. More than 40 years later, Golden et al. (2012) offered examples of sensors and microfluidic devices that use flow focusing to control the cross section of a sample stream. A case of asymmetrical focusing was studied experimentally and numerically by Carlotto et al. (2010). The experimental and numerical study done by Kennedy et al. (2009) used a 3D manifold for vertical positioning of the focused sample, and Lee et al. (2009) obtained 3D focusing with only one sheath of fluid using contraction–expansion sequences. The same effect was also achieved by Lin et al. (2012) using a straight channel with two vertical inlets in order to have a single layer and single sheath flow. Particle focusing in a straight microchannel was achieved by Fan et al. (2014) using asymmetrical sharp corners on one side of the wall. Their presence generates vortices that play a role in the balance between inertial lift effects and centrifugal forces. Bhagat et al. (2008) studied the migration of particles in rectangular channels and the equilibrium positions that these will reach in relation to the forces that act upon them.

Brennich and Köster (2013) demonstrated that a smaller height of the main channel leads to a longer reaction time between two fluid streams. They examined the effects of diffusion and reaction time. Ion concentration gradients in a nanochannel were studied by Hsu et al. (2014), due to the importance of chemical species concentrations inside channels used in different applications.

Zhang et al. (2008) studied the mixing performance due to the focusing effect in a double *Y* microchannel.

Kunstmann-Olsen et al. (2011) investigated the influence of the confluence angle between channels and of the volumetric flow rate ratio on the hydrodynamic focusing phenomenon in a three inlet junction having the branches positioned at 45°, 67.5° and 90° angles. The conclusion was that a 90° orientation of the inlets leads to the narrowest focused stream. Nasir et al. (2011) investigated experimentally (with confocal microscopy and the PIV method) and numerically the parameters (angle, Reynolds number, and channel cross section and symmetry) affecting the shape of a hydrodynamically focused stream. The authors used a microchannel with two inlets (90°—*T* and 45°—*Y* configurations) and one outlet.

The control of the flow inside the microchannel can be done by either adjusting the pressure (Hoffmann et al. 2006; Iliescu et al. 2014) or the flow rate (Zhang et al. 2008; Ushikubo et al. 2014). It is well known that by increasing the pressure or flow rate for the sheath fluid, the sample fluid stream becomes narrower. By contrast, particle focusing can also be achieved by cross-stream migration in curved channels using Dean vortices (Ha et al. 2014).

Jahn et al. (2007) studied the effect of channel aspect ratio on the size distribution of liposomes produced by flow focusing. They reported that rectangular channels of high aspect ratio are more adequate than trapezoidal channels. This is useful when the reduction in surface effects at the top and bottom walls is desired. In addition to this, they presented a theoretical model for calculating the minimum width of the focused stream. In a later work, Jahn et al. (2013) investigated new techniques like freezing for instantaneous immobilization to visualize the liposome assembly in microchannels. Mijajlovic et al. (2013) used a cross-shaped microchannel geometry to elucidate the effect of certain parameters on the size distribution of liposomes.

The hydrodynamic focusing phenomenon can also be utilized to control and induce conformational changes of DNA molecules (Iliescu et al. 2014).

As it was previously observed (Wong et al. 2004), the flow in channels separates in the vicinity of discontinuities, like sharp angles of the walls. The streams with higher velocity tend to flow toward the outlet, due to inertial forces, while the fluid boundary layer will turn and follow the channel walls. This kind of flow pattern occurs in micromixers, which are usually microchannels with at least two inlets and one outlet. Their geometries can vary from *Y*, *T*, or cross-shaped to complex ramifications, with straight or curved channels, smooth or patterned walls.

A common feature of some micromixers and the subject matter studied in this work is the occurrence of vortex patterns at channel junctions. An analysis of the enhanced mixing by means of a pair of vortices was presented by Wong et al. (2004), Kockmann et al. (2006), and Engler et al. (2004) in a *T*-shaped micromixer. Bothe et al. (2006, 2011) observed the formation of a pair of symmetrical vortices at a critical Reynolds number. Similar experimental and numerical studies have been performed by Hoffmann et al. (2006), Kockmann et al. (2007), and Soleymani et al. (2008).

The presence of vortices in microfluidic devices not only enhances mixing, but also helps trapping cells or particles in a specific region of the microchannel. This assists in separating specific components from a fluid stream. Zhou et al. (2013) identified a critical value of the Re number that leads to particle recirculation in the vortex. They also analyzed the influence of particle concentration on the separation performance.

Although a lot of research has been done on hydrodynamic focusing and its influence on controlling the position of a fluid stream, the onset of vortex formation in the junction area was investigated and analyzed only in very few papers. Oliveira et al. (2012) performed a detailed 2D numerical analysis of the flow patterns in a cross-microgeometry with three entrances and one exit. The authors also compared 3D numerical results with direct flow visualizations and obtained the conditions for the onset of the vortical structures within the junction. More recently, Haward et al. (2016) presented numerical and experimental investigations of the spiral vortex formation in a cross-slot domain with two entrances and two exits.

The goal of the current study is to investigate the case of extreme focusing in a domain with three entrances and one exit, accompanied by the formation and evolution of two symmetrical counter-rotating vortices in the junction region. The vortices split the fluid stream to be focused into four individual streams close to the corners of the microchannel. Understanding and characterizing the stream formation due to the narrow focusing and the presence of vortices at the junction area could be a first step in developing new applications based on the manipulation and control of sample streams.

2 Materials and methods

2.1 Experimental setup and protocol

The experimental setup is based on microscopy imaging of the flow patterns inside a microfluidic chip. The visualizations were performed mostly in fluorescence mode using an inverted microscope (Nikon Eclipse Ti, Nikon GmbH, Düsseldorf, Germany). The fluid used in the experiments was deionized water (Millipore Milli-Q A10, Molsheim, France). In order to observe the evolution of the flow focusing and the formation of the vortical structures, the water entering the main inlet of the microfluidic chip was dyed with rhodamine B isothiocyanate (Sigma-Aldrich, Chemie GmbH, Taufkirchen, Germany) at a concentration of 0.04% (w/v), low enough to not significantly influence the fluid properties. The illumination source was a Melles Griot He–Ne Laser (Melles Griot GmbH, Bensheim, Germany) with an excitation wavelength of 543 nm. The image recording was carried out with a CCD camera (Andor iXon, Oxford Instruments, Belfast, UK) mounted on the microscope, and the images were processed with the NIS Elements AR software.

The microchannels were fabricated in a silicon wafer using Deep Reactive Ion Etching (DRIE), Bosch process. An inductively coupled plasma (ICP) system (Oxford Instruments, Bristol, UK) was used to etch the microgeometry and the backside holes for the inlets and outlet. This technique allows to obtain vertical side walls of the microchannels and sharp corners in the junction area. The design and dimensions of the microchannels are presented in Fig. 1 and are similar to what was used by Oliveira et al. (2012).

The microfluidic chip was sealed with a borosilicate glass slide by anodic bonding. This ensures a transparent cover for the visualizations. In order to provide fluid connections to the device, Nanoport (Upchurch Scientific, Oak Harbor, USA) connectors and PTFE tubing (Sigma-Aldrich, Chemie GmbH, Taufkirchen, Germany) (inner diameter 0.56 mm) were attached at the access points for inlets and outlet.

The flow dynamics was also investigated using laser scanning confocal microscopy (LSCM) with a 20× objective. This offers a 3D view of the hydrodynamic focusing phenomenon and vortex structure. Apart from the confocal mode, the microscope can also be operated in epifluorescence mode. The smallest pinhole (30 µm) available for the confocal microscope was chosen. The z-scanning was done with a step size of 2.5 µm, and the x–y slices were acquired at 0.5 fps with a resolution of 1024 × 1024 pixels.

The design displayed in Fig. 1 has three inlets and one outlet. The two symmetrical lateral branches i_{21} and i_{22} (with a common secondary inlet i_2) are perpendicular at the junction to the main channel with inlet i_1. All microchannels have a square cross section of 100 µm × 100 µm.

In order to maintain a stable flow through the microfluidic chip, a pressure-controlled pump (ElveFlow, Paris, France) was used. It has two pressure ports equipped with flow rate sensors, one for each inlet of the microfluidic device. At the first port, the value of the pressure can be maintained constant in the range 0–200 mbar, while for the second port the range is 0–2000 mbar. The pump was controlled by a computer via USB connection, and the pressure was monitored with the ElveFlow Smart Interface software. The pressure and flow rate data from the sensors were recorded with a time step of 0.1 s and then exported to an Excel Sheet.

In the experiments, the pressure p_1 at the main inlet i_1 was increased from 100 to 200 mbar in steps of 5 mbar. For each pressure step imposed at the main inlet, at the secondary inlet the applied pressure p_2 was increased accordingly in steps of 1 mbar, in order to observe the transition between different flow regimes inside the junction. Each pair of input parameters (p_1, p_2) was kept constant for 7 s before a new acquisition; during this time, no variation of the observed flow pattern occurred. Each experiment was repeated twice in order to

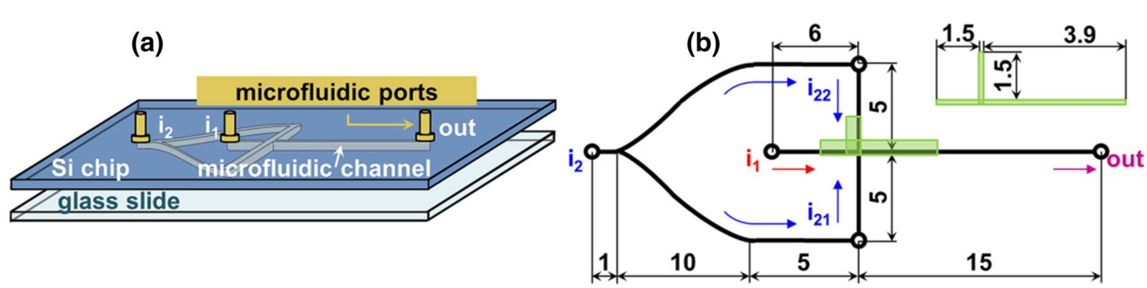

Fig. 1 **a** Schematic of the microfluidic chip. **b** Design and dimensions (in mm) of the microchannel network used in the experiments with the area of interest used in the numerical simulations indicated in *green*. The cross section of the microchannels is 100 µm × 100 µm (color figure online)

ensure the reproducibility of the results. In each experiment, the correlation between the flow pattern and the data from the pump was established by acquiring the data simultaneously.

From the symmetry of the geometry (as can be seen in Fig. 1), one can infer the symmetry of the flow rate Q:$Q_{21} = Q_{22} = Q_2/2$, (i.e., $\mathrm{Re}_{21} = \mathrm{Re}_{22} = \mathrm{Re}_2/2$) and of the input pressure p:$p_{21} = p_{22} = p_2$, where the subscripts refer to the corresponding branches/inlets. The experimental observations indicate a symmetrical flow pattern with respect to the symmetry plane in the main channel and therefore support the assumption of splitting into two equal substreams. The Reynolds number was calculated with the formula

$$\mathrm{Re} = \frac{\rho V_0 D_h}{\eta}, \tag{1}$$

where ρ and η represent the density and the viscosity of the fluid, V_0 is the mean velocity at the inlet of the channel, and $D_h = 4A/P$ is the hydraulic diameter (here A is the cross-sectional area and P is the wetted perimeter).

The fluid introduced through i_1 is focused in the main channel downstream of the junction, with a flow pattern dependent on the Reynolds number in the main channel $\mathrm{Re}_{\mathrm{out}} = \mathrm{Re}_1 + \mathrm{Re}_2$ and the flow rate ratio Q_1/Q_{22}.

2.2 Numerical simulations

The numerical simulations were performed based on a finite-volume code implemented in the commercial solver ANSYS-Fluent.

We have solved the Navier–Stokes equation and the continuity equation for an incompressible fluid in the absence of a body force:

$$\rho\left(\frac{\partial \boldsymbol{v}}{\partial t} + (\boldsymbol{v}\cdot\boldsymbol{\nabla})\boldsymbol{v}\right) = -\boldsymbol{\nabla} p + \eta \Delta \boldsymbol{v} \qquad \boldsymbol{\nabla}\cdot\boldsymbol{v} = 0 \tag{2}$$

where $\boldsymbol{v}$ is the velocity vector and p is the pressure.

The SIMPLE pressure-correction scheme was used, and the momentum equation was discretized based on a first-order upwind scheme. A time step of 10^{-6} s was chosen for the calculations. The numerical procedure is further detailed in Bălan et al. (2012), see also (Anderson et al. 2009; Wesseling 2001; Ferziger and Peric 2002; Fluent 6.3 User's Manual 2006).

We also performed numerical computations of the steady-state solution. The final results are identical to the transient ones after 700 time steps. Therefore, the formation time of the velocity profile is about 0.7 ms.

The computational mesh consisted of hexahedral finite volumes, and a representative detail is shown in Fig. 2. The convergence criteria (absolute) for the solution of the Navier–Stokes equation were set as 10^{-8}, representing the ratio between the highest value of the error (calculated in the center of all cells) for the current iteration and the error obtained at the first iteration. In the case of the continuity equation, this criterion is calculated by dividing the result of the error for the current iteration to the average obtained from the first five errors. The simulations were performed for a single fluid phase, water, with constant density ($\rho = 998.2$ kg/m^3) and viscosity ($\eta = 0.001$ Pa s), at constant temperature ($\theta = 20$ °C).

The dimensions of the model flow domain, c.f. Fig. 1, were chosen in such a manner to capture the important flow features corresponding to the four cases from Table 1. Thus, the channel junction in Fig. 1 was modeled, with inlet and outlet channels of a length of 1.5 and 3.9 mm, respectively. The flow develops into a stable close-to-parabolic velocity profile about 75 µm away from the entrance, which indicates that the inlet branches of the model are long enough.

The imposed boundary conditions are indicated as follows: constant velocity at the inlets (i_1 and i_{22}), zero relative pressure at the outlet of the channel and zero velocity at the walls. The symmetry of the microchannel domain and the boundary conditions was exploited by defining a plane with a symmetry boundary condition. The computational domain

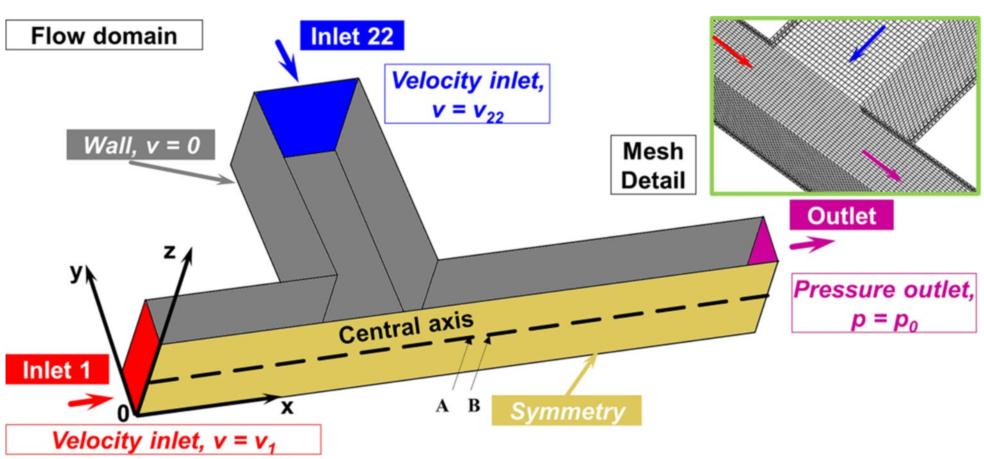

Fig. 2 Computational domain with the imposed boundary conditions. The points A and B located on the central axis immediately downstream of the junction indicate the x-coordinates that define the interval where the variations of the velocity magnitude and pressure were investigated for the mesh independence study of Fig. 3

Table 1 Numerically investigated cases with the corresponding input parameters

Case	p_1 (mbar)	v_1 (m/s)	v_{22} (m/s)	Re_{out} (−)	Q_1/Q_{22} (−)
Focusing	100	0.00483	0.205	41.60	0.0235
Vortex	100	0.0005	0.209	41.95	0.00238
Focusing	200	0.0305	0.388	80.8	0.079
Vortex	200	0.00216	0.411	82.6	0.00525

Table 2 Number of cells corresponding to the used meshes

Mesh Nr.	No. of cells
M1	359,424
M2	822,382
M3	1,804,164
M4	118,874
M5	681,250
M6	1,137,500

with the appropriate boundary conditions is presented in Fig. 2.

For validation of the numerics and comparison with the experimental data, four different cases were studied. The four analyzed cases, with the appropriate input parameters and calculated Reynolds numbers, are presented in Table 1.

Several structured meshes were analyzed in order to establish the optimal one. The number of cells is given in Table 2. M1, M2, and M3 have a more refined discretization toward the wall faces compared to the bulk domain, while M4, M5, and M6 were generated with constant cell dimension; M6 has twice the number of cells in the main channel in comparison with the side channels.

A comparison between the results computed with the six different meshes is shown in Fig. 3 for Case 4 from Table 1. This case corresponds to the presence of a vortex inside the microchannel. In Fig. 3, the velocity and pressure magnitudes are plotted along the central axis of the main channel.

From Fig. 3, it can be concluded that, with the exception of the M4 mesh, the results are very similar. Only in the blowup of the region where steep gradients occur, some differences are visible. Given the fact that the region of interest is the junction area, we further proceeded with the numerical analysis using M6. This option offers a reasonable computational time (21 min for the steady solution and 4 h and 21 min for the unsteady solution up to a simulation time of 700 ms) with the available resources (3 GHz CPUs, 2 processors, 8 cores, 128 GB RAM).

3 Experimental results

For visualization of the flow inside the cross-shaped microfluidic device, a dye was added to the stream entering through inlet i_1 and the spatial distribution of that dye was recorded through epifluorescence and confocal microscopy. Particular attention was given to the transition between the flow focusing pattern and a flow pattern with a pair of counter-rotating vortices in the junction area.

Qualitatively, the transition between these flow patterns proceeds as follows when decreasing the ratio of the flow through inlet i_1 and the flow through the side branches. In the median plane, the fluid reaches a focusing length (l_f) after which it splits into two secondary jets, directed by the secondary fluid from the side channels toward the top and bottom walls of the main channel. The left-hand side of Fig. 4a depicts the flow structure of the fluid originating from the median plane in the main inlet channel. The frame at the center shows streamlines that have been distributed over the entire cross section of the main inlet channel. The right-hand side of Fig. 4a serves to give a definition of the parameters characterizing the flow structures. As the flow rate Q_1 is decreasing, at a critical value of Q_1/Q_{22} (which defines the transition point) a vortex develops that splits the flow into four streaks close to the corners of the main channel as it can be observed in Fig. 4b, which is organized in

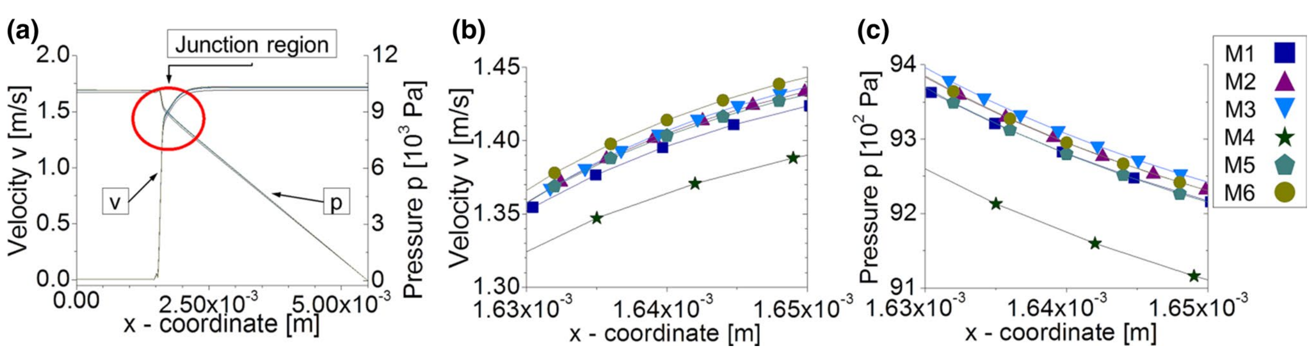

Fig. 3 Results of the mesh influence study; **a** pressure and velocity variation along the central axis of the main channel with details of velocity (**b**) and pressure (**c**) in the junction region. On the scale of part **a** the results obtained with different meshes are indistinguishable

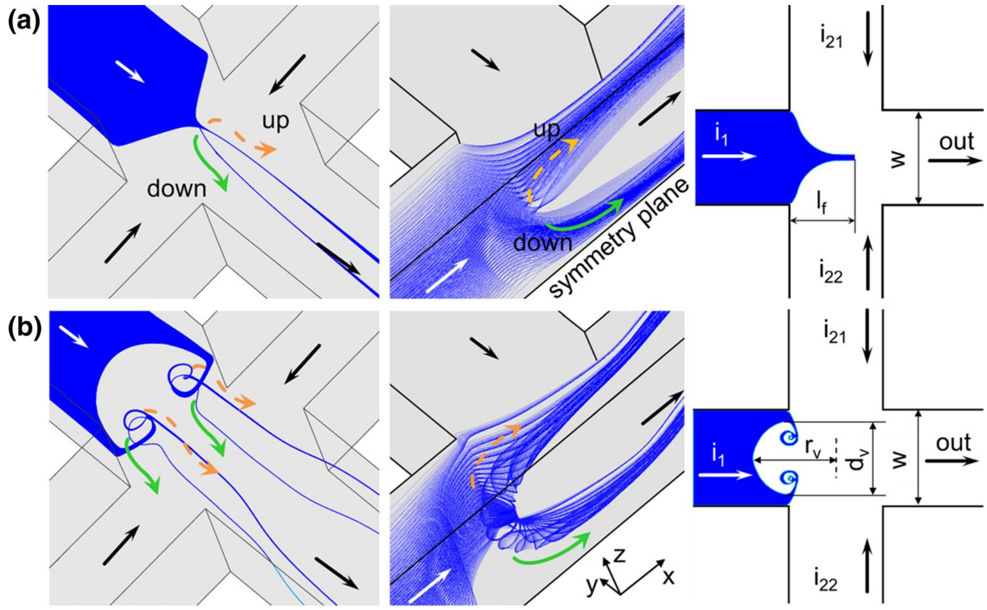

Fig. 4 Flow patterns close to the transition point where vortices develop. The *dashed arrows* indicate streaks ending up close to the *top wall*, the *solid arrows* streaks ending up close to the *bottom wall*. **a** Focused stream splitting into two fluid streaks; **b** vortex structures splitting into four fluid streaks

the same way as Fig. 4a. The generated flow structure is similar to a "vortex ring" with a "mushroom" shape defined by a radius r_v (measured from the center of the junction) and the diameter d_v, which represents the width of the vortex. This structure will grow in size with increasing Reynolds numbers Re_{21} and Re_{22}. A qualitative sketch of the two corresponding flow patterns is presented in Fig. 4.

The main goal of the experimental study was to correlate the flow pattern at the channel junction with the Reynolds number in the outlet channel and the ratio of the flow rates at the inlets.

For the two cases shown in Fig. 4, the characteristic features of the flow patterns in the median plane were measured. These experimental findings are later used to validate the results from the numerical simulations.

In order to create a flow pattern map, experiments at various Reynolds numbers and flow rate ratios were performed. The flow inside the junction domain is symmetrical if the flow rates of fluid 2 from the entrances i_{21} and i_{22} are identical. This is the case for the present investigation.

The flow pattern map including fluorescence micrographs of the region where the transition occurs is shown in Fig. 5.

The map represents in the parameter space spanned by Re_{out} and Q_1/Q_{22} the transition between flow focusing and vortex formation. Each dot in the graph corresponds to one experiment. The control of the flow inside the chip was done by maintaining a selected pressure at the inlets. Thus, by increasing the pressure controlling the flow in the secondary branches, the flow rate in the main channel decreases. In this way, the Reynolds number in the outlet channel of the device slightly increases for each set of experiments from right to left. There are 21 sets of values of Re_{out} for which we investigated the flow patterns, in the range $Re_{out} \in [40, 85]$. Three zones are identified: **zone I**—a narrow flow focusing in the median plane (the "classical" uniform flow focusing that has been intensely investigated in the previous studies mentioned in Introduction), **zone II**—a transition region between focusing and the formation of vortices and **zone III**—the development of a well-defined pair of counter-rotating vortices (see also the sketch from Fig. 4).

The boundary between zones II and III was obtained by Oliveira et al. (2012) in a similar flow classification map, which was constructed based on numerical results (up to $Re_{out} \cong 350$). Even though the investigated range of the Reynolds numbers is different, the numerical results by Oliveira et al. (2012) agree quantitatively with our experimental findings, obtained for outlet Reynolds numbers between 40 and 85.

The data points where the flow focusing into a stream in the median plane of the channel stops are encircled. A dashed line has been introduced to connect these points. To the left of this line, the fluid stream from inlet i_1 is split by the faster flowing fluid from inlet i_2. It is then redirected toward the top and bottom walls of the geometry, as confocal microscopy measurements demonstrated.

There exists a transition region (zone II) between the flow focusing region and the onset of a vortex structure, where the focusing into a single streak is replaced by vortical flows leading to multiple streaks. In zone III, a pair of counter-rotating vortices is clearly visible and fully developed. The points marking the transition between zones II and III are indicated with squares, connected by a solid line. Zone III grows in size with the increase in the outlet Reynolds number. The diameters and radii of a vortex, as defined in Fig. 4, are indicated in the caption of Fig. 5 for both zone II and zone III. With the employed experimental setup, it was not

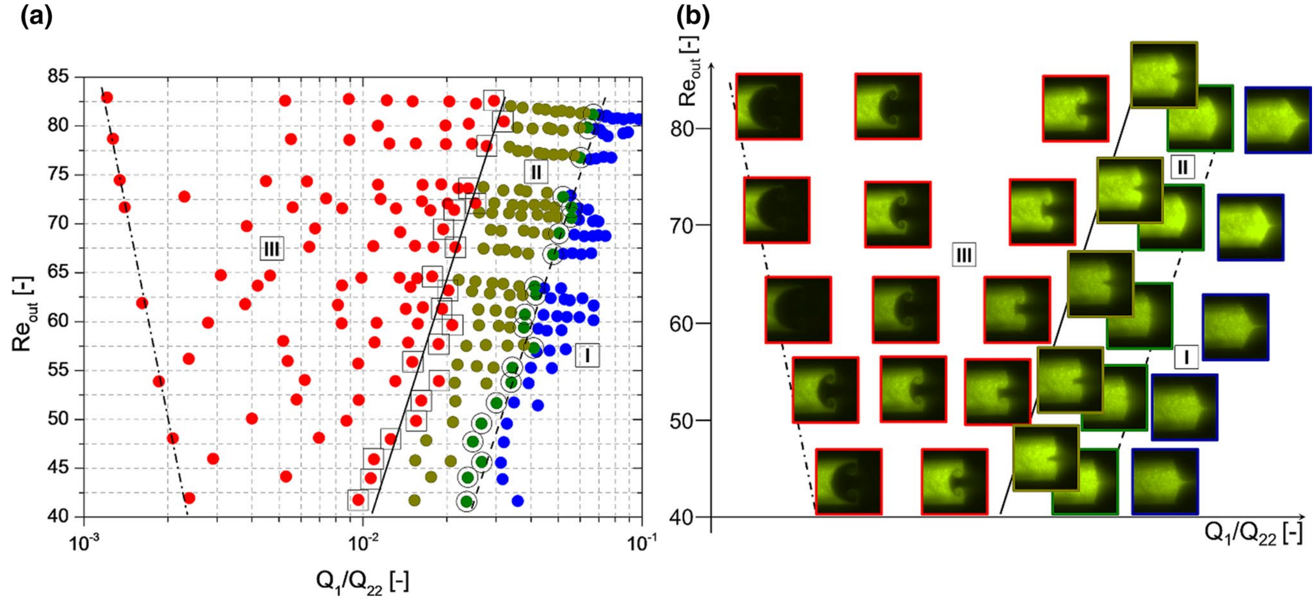

Fig. 5 Flow pattern map describing the local hydrodynamics in the junction area of a cross-shaped flow focusing microchannel. **a** Experimental data points in the $(\mathrm{Re}_{\mathrm{out}}, Q_1/Q_{22})$ plane, colored according to the type of flow pattern. A transition region (**zone II**) is present between narrow focusing (**zone I**) and the formation of "vortex rings" (**zone III**). The characteristic values of the parameters r_v, d_v and l_f are as follows. Zone I: $l_f \in [25\,\mu\mathrm{m}, 60\,\mu\mathrm{m}]$; Zone II: $r_v \in [0, 60\,\mu\mathrm{m}], d_v \in [0, 45\,\mu\mathrm{m}]$; Zone III: $r_v \in [60\,\mu\mathrm{m}, 110\,\mu\mathrm{m}], d_v \in [45\,\mu\mathrm{m}, 95\,\mu\mathrm{m}]$. **b** Fluorescence micrographs indicating the structure of the flow patterns in different regions of the parameter space

possible to decrease Q_1/Q_{22} below the values marked by the dashed-dotted line. Beyond that line, a backward flow through inlet i_1 was observed.

3.1 Comparison between experiments and simulations

To further corroborate the findings reported in the previous section, the experimental results were compared to the results from the numerical simulations. A qualitative comparison between numerics and experiments is shown in Fig. 6, indicating a good agreement between the two data sets. A more detailed representation of the 3D flow structures is shown in Fig. 7.

A quantitative validation of the numerical simulations is obtained by measuring the geometrical parameters described in Fig. 5: (1) the length l_f of the jet in the junction region and (2) the quantities d_v and r_v characterizing the shape of the vortex. The results are presented in Table 3.

A reasonable agreement between the three data sets is observed. One can observe that deviations between the values from simulations and confocal microscopy are larger than those between the values from simulations and epifluorescence microscopy. This fact is explained by the larger

Fig. 6 Comparison between the results of numerical simulations (**a**) and epifluorescence microscopy (**b**) for all four cases indicated in Table 1

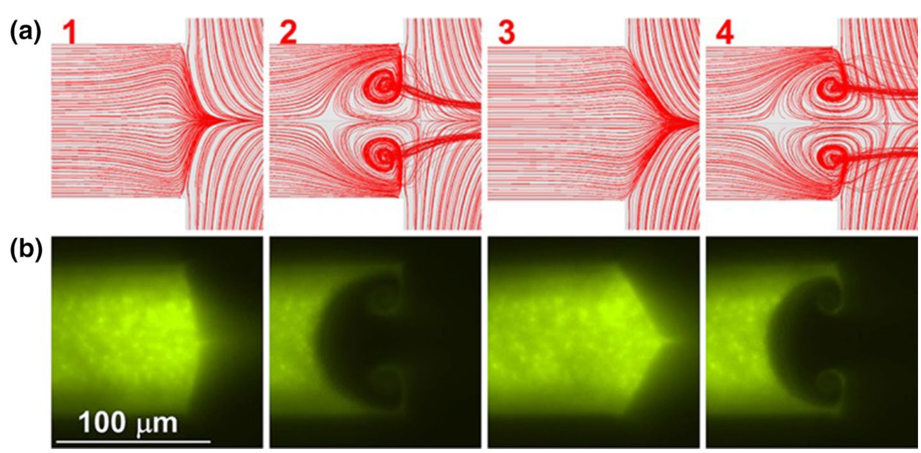

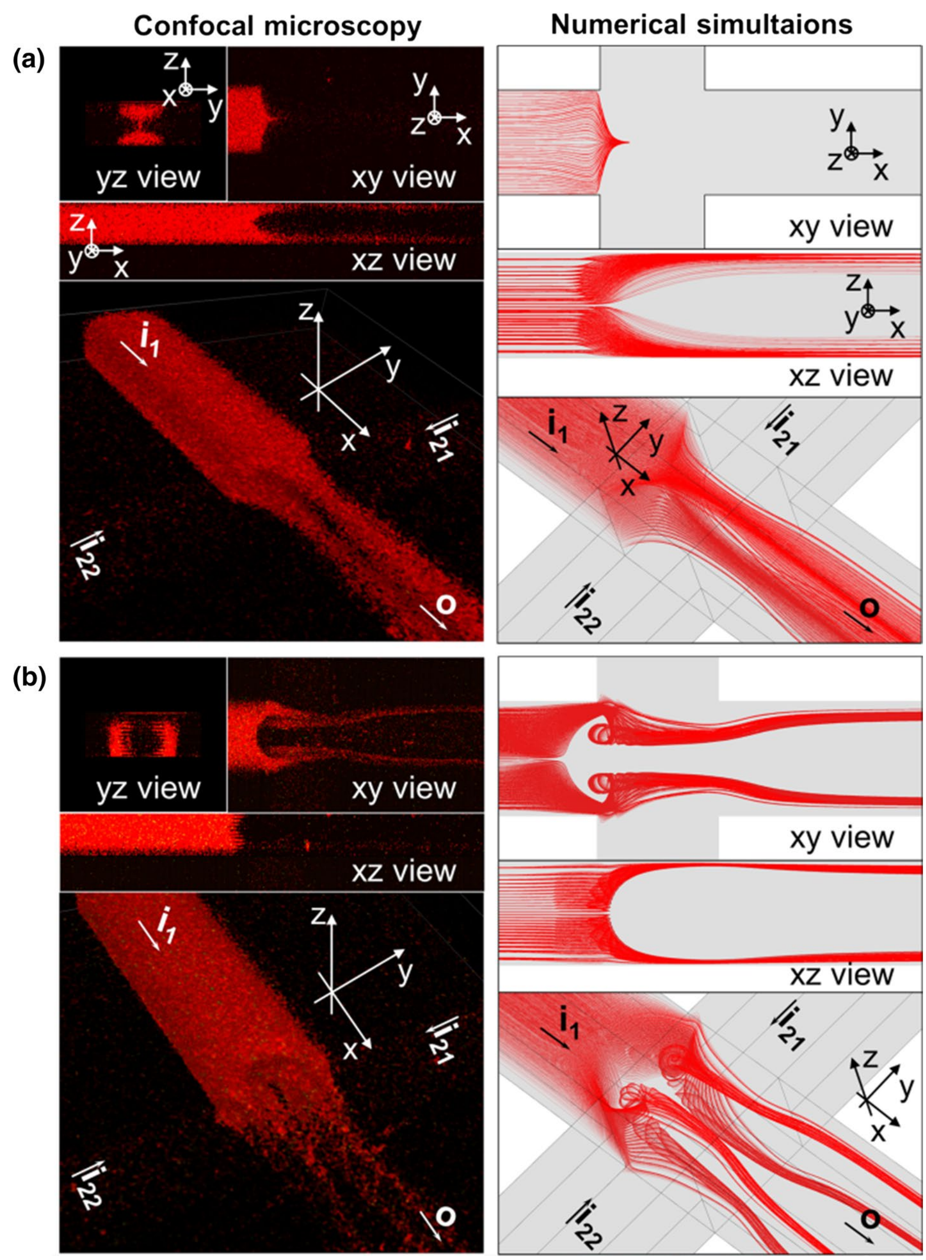

Fig. 7 3D images of flow patterns. *Left column* confocal microscopy visualizations; *right column* numerical simulations. Section **a** corresponds to Case 1 (Re_{out} = 40), section **b** to Case 4 (Re_{out} = 80)

photon count of epifluorescence microscopy which generates less noisy images, so a more precise visualization of the flow patterns is possible. Also, the fact that the flow is controlled by the input pressure (instead of the flow rates, which are measured) might lead to some errors in the computation of the average velocity.

In the case of flow focusing, we analyzed the results for two cases, Re_{out} = 40 and Re_{out} = 80 (Cases 1 and 4), see Fig. 7. The higher Re_{out}, the more elongated is the fluid stream. As already depicted in Fig. 4, in Case 1 the incoming flow through inlet i_1 splits into two streams close to the top and the bottom wall of the outlet channel. In Case 4, the numerical results confirm the jet splitting into four streams close to the corners in the outlet channel. The splitting of the stream entering through inlet i_1 into narrow streams close to the corners in the outlet channel has already been noticed by Oliveira et al. (2012). By contrast, the pattern with two streams close to the top and the bottom wall of the outlet channel does not appear to have been identified up to now.

The numerical simulations offer a correct representation of the flow field. Therefore, in view of potential applications one can extract from the computed results kinematic and dynamic quantities of interest such as the residence time of particles inside the junction, the spatial distribution of the vorticity, or the values of the wall shear stress. Also the present results may be utilized to more precisely direct samples to specific locations inside the channel, or to achieve inertial

Table 3 Quantitative comparison between experimental results from epifluorescence microscopy (EPI), confocal microscopy (C.M.), and numerical simulations for flow focusing and vortex formation cases. The geometrical parameters were measured using the ImageJ software

	d_v (μm)	r_v (μm)	l_f (μm)
$Re_{out} \cong 40$			
Focusing (1)			
EPI	–	–	21.3
N.S.	–	–	23.1
C.M.	–	–	24.3
$Re_{out} \cong 80$			
Focusing (3)			
EPI	–	–	43.2
N.S.	–	–	44.1
C.M.	–	–	36.8
Vortex (4)			
EPI	94.4	84.8	–
N.S.	91.9	81.1	–
C.M.	80	71.2	–

particle sorting by exploiting their different abilities to follow the streamlines of the flow.

4 Conclusions

We have studied the local hydrodynamics in the junction area of a flow focusing microfluidic device. The study was mainly directed to the numerical modeling and experimental investigation of the formation of vortical structures. A comprehensive description and characterization of the flow patterns is obtained by correlating the flow visualizations with numerical results.

The experimental results, derived from epifluorescence and confocal microscopy visualizations, are found to be consistent with the 3D numerical simulations. A flow pattern map in the space spanned by the characteristic Reynolds number and the flow rate ratio has been obtained in which three zones are identified: Zone I—a flow focusing scenario producing one focused fluid stream in the outlet channel, zone II—a transition region between focusing and the formation of a flow pattern with vortices, and zone III—the development of a well-defined pair of counter-rotating vortices.

In zone I, the flow is focused into one stream covering the median plane of the outlet channel. During the transition (zone II), the number of streams originating from the flow through the main inlet increases. In zone III, due to the presence of vortices, the fluid flowing through the main channel is split into four streams that are redirected toward a position close to the corners of the outlet channel. Between these two regimes, a situation emerges where the flow is focused into two streams close to the upper and lower wall of the outlet channel.

The obtained results expand the possibilities of flow focusing devices for applications in microfluidics. In particular, interesting in that context appears the possibility of selecting the number of outlet streams and their position downstream of the junction. Also, it will be worth exploring the potential of the described flow patterns for inertial particle sorting/separation and the control of their residence time. For example, it is conceivable that small particles inside the main channel get redirected by the vortices to streams close to the corners of the outlet cross section, whereas large particles for which inertia plays a bigger role are not able to follow the streamlines. This would enable a novel type of inertial particle sorting/separation.

Acknowledgements The authors acknowledge Dr. eng. Catalin Marculescu for his assistance in fabrication of the microchannels and also the financial support received from the grant UEFISCDI, projects PN-II-ID-PCE-2012-4-0245/2013 and PN-II-PT-PCCA-2011-3.1-0052. The work of Iulia Rodica Damian was funded by the Sectoral Operational Programme Human Resources Development 2007–2013 of the Ministry of European Funds through the Financial Agreement POSDRU/159/1.5/S/132397.

References

Anderson JD, Degroote J, Degrez G, Dick E, Grundmann R, Vierendeels J (2009) Computational fluid dynamics. Springer, Berlin. doi:10.1007/978-3-540-85056-4

Bălan CM, Broboană D, Bălan C (2012) Investigations of vortex formation in microbifurcations. Microfluid Nanofluid 13:819–833. doi:10.1007/s10404-012-1005-8

Bhagat AAS, Kuntaegowdanahalli SS, Papautsky I (2008) Inertial microfluidics for continuous particle filtration and extraction. Microfluid Nanofluid 7:217–226. doi:10.1007/s10404-008-0377-2

Bothe D, Stemich C, Warnecke HJ (2006) Fluid mixing in a T-shaped micro-mixer. Chem Eng Sci 61:2950–2958. doi:10.1016/j.ces.2005.10.060

Bothe D, Lojewski A, Warnecke HJ (2011) Fully resolved numerical simulation of reactive mixing in a T-shaped micromixer using parabolized species equations. Chem Eng Sci 66:6424–6440. doi:10.1016/j.ces.2011.08.045

Brennich ME, Köster S (2013) Tracking reactions in microflow. Microfluid Nanofluid 16:39–45. doi:10.1007/s10404-013-1212-y

Carlotto S, Fortunati I, Ferrante C, Schwille P, Polimeno A (2010) Time correlated fluorescence characterization of an asymmetrically focused flow in a microfluidic device. Microfluid Nanofluid 10:551–561. doi:10.1007/s10404-010-0689-x

Engler M, Kockmann N, Kiefer T, Woias P (2004) Convective mixing and its applications to micro reactors. In: Proceedings of ICMM2004-2412. pp 781–788. doi: 10.1115/ICMM2004-2412

Fan L-L, Han Y, He X-K, Zhao L, Zhe J (2014) High-throughput, single-stream microparticle focusing using a microchannel with asymmetric sharp corners. Microfluid Nanofluid 17:639–646. doi:10.1007/s10404-014-1344-8

Ferziger JH, Peric M (2002) Computational methods for fluid dynamics. Springer, Berlin. doi:10.1007/978-3-642-56026-2

FLUENT6.3 Doc. User's Manual, 2006 Fluent Incorporated, Lebanon, New Hampshire

Fu T, Wu Y, Ma Y, Li HZ (2012) Droplet formation and breakup dynamics in microfluidic flow-focusing devices: from dripping to jetting. Chem Eng Sci 84:207–217. doi:10.1016/j.ces.2012.08.039

Golden JP, Justin GA, Nasir M, Ligler FS (2012) Hydrodynamic focusing-a versatile tool. Anal Bioanal Chem 402:325–335. doi:10.1007/s00216-011-5415-3

Ha BH, Lee KS, Jung JH, Sung HJ (2014) Three-dimensional hydrodynamic flow and particle focusing using four vortices Dean flow. Microfluid Nanofluid. doi:10.1007/s10404-014-1346-6

Haward SJ, Poole RJ, Alves MA, Oliviera PJ, Goldenfeld N, Shen AQ (2016) Tricritical spiral vortex instability in cross-slot flow. Phys Rev E 93:031101(R). doi:10.1103/PhysRevE.93.031101

Hoffmann M, Schlüter M, Räbiger N (2006) Experimental investigation of liquid-liquid mixing in T-shaped micro-mixers using µ-LIF and µ-PIV. Chem Eng Sci 61:2968–2976. doi:10.1016/j.ces.2005.11.029

Hong JS, Stavis SM, Depaoli Lacerda SH, Locascio LE, Raghavan SR, Gaitan M (2010) Microfluidic directed self-assembly of liposome-hydrogel hybrid nanoparticles. Langmuir 26:11581–11588. doi:10.1021/la100879p

Hsu WL, Inglis DW, Jeong H, Dunstan DE, Davidson MR, Goldys EM, Harvie DJE (2014) Stationary chemical gradients for concentration gradient-based separation and focusing in nanofluidic channels. Langmuir 30:5337–5348. doi:10.1021/la500206b

Iliescu C, Mărculescu C, Venkataraman S, Languille B, Yu H, Tresset G (2014) On-Chip Controlled Surfactant–DNA Coil-Globule Transition by Rapid Solvent Exchange Using Hydrodynamic Flow Focusing. Langmuir 30:13125–13136. doi:10.1021/la5035382

Jahn A, Vreeland WN, Devoe DL, Locascio LE, Gaitan M (2007) Microfluidic directed formation of liposomes of controlled size. Langmuir 23:6289–6293. doi:10.1021/la070051a

Jahn A, Lucas F, Wepf RA, Dittrich PS (2013) Freezing continuous-flow self-Assembly in a microfluidic device: toward imaging of liposome formation. Langmuir 29:1717–1723. doi:10.1021/la303675g

Kennedy MJ, Stelick SJ, Perkins SL, Cao L, Batt CA (2009) Hydrodynamic focusing with a microlithographic manifold: controlling the vertical position of a focused sample. Microfluid Nanofluid 7:569–578. doi:10.1007/s10404-009-0417-6

Kockmann N, Kiefer T, Engler M, Woias P (2006) Convective mixing and chemical reactions in microchannels with high flow rates. Sens Actuators B Chem 117:495–508. doi:10.1016/j.snb.2006.01.004

Kockmann N, Dreher S, Woias P (2007) Unsteady laminar flow regimes and mixing in T-shaped micromixers. In: ASME 5th international conference on nanochannels, microchannels, minichannels. pp 671–678. doi: 10.1115/ICNMM2007-30041

Kunstmann-Olsen C, Hoyland JD, Rubahn H-G (2011) Influence of geometry on hydrodynamic focusing and long-range fluid behavior in PDMS microfluidic chips. Microfluid Nanofluid 12:795–803. doi:10.1007/s10404-011-0923-1

Lee MG, Choi S, Park J-K (2009) Three-dimensional hydrodynamic focusing with a single sheath flow in a single-layer microfluidic device. Lab Chip 9:3155–3160. doi:10.1039/b910712f

Lin S-C, Yen P-W, Peng C-C, Tung Y-C (2012) Single channel layer, single sheath-flow inlet microfluidic flow cytometer with three-dimensional hydrodynamic focusing. Lab Chip 12:3135. doi:10.1039/c2lc40246g

Maenaka H, Yamada M, Yasuda M, Seki M (2008) Continuous and size-dependent sorting of emulsion droplets using hydrodynamics in pinched microchannels. Langmuir 24:4405–4410. doi:10.1021/la703581j

Mijajlovic M, Wright D, Zivkovic V, Bi JX, Biggs MJ (2013) Microfluidic hydrodynamic focusing based synthesis of POPC liposomes for model biological systems. Colloids Surfaces B Biointerfaces 104:276–281. doi:10.1016/j.colsurfb.2012.12.020

Nasir M, Mott DR, Kennedy MJ, Golden JP, Ligler FS (2011) Parameters affecting the shape of a hydrodynamically focused stream. Microfluid Nanofluid 11:119–128. doi:10.1007/s10404-011-0778-5

Oliveira MSN, Pinho FT, Alves MA (2012) Divergent streamlines and free vortices in Newtonian fluid flows in microfluidic flow-focusing devices. J Fluid Mech 711:171–191. doi:10.1017/jfm.2012.386

Rodriguez-Trujillo R, Mills CA, Samitier J, Gomila G (2006) Low cost micro-Coulter counter with hydrodynamic focusing. Microfluid Nanofluid 3:171–176. doi:10.1007/s10404-006-0113-8

Rondeau E, Cooper-White JJ (2008) Biopolymer microparticle and nanoparticle formation within a microfluidic device. Langmuir 24:6937–6945. doi:10.1021/la703339u

Schabas G, Yusuf H, Moffitt MG, Sinton D (2008) Controlled self-assembly of quantum dots and block copolymers in a microfluidic device. Langmuir. doi:10.1021/la703297q

Soleymani A, Kolehmainen E, Turunen I (2008) Numerical and experimental investigations of liquid mixing in T-type micromixers. Chem Eng J 135:219–228. doi:10.1016/j.cej.2007.07.048

Spielman G, Goren SL (1968) Improving Resolution in Coulter Counting by Hydrodynamic Focusing. J Colloids Interface Sci 26:175–182

Ushikubo FY, Birribilli FS, Oliveira DRB, Cunha RL (2014) Y- and T-junction microfluidic devices: effect of fluids and interface properties and operating conditions. Microfluid Nanofluid 17:711–720. doi:10.1007/s10404-014-1348-4

Wang WH, Zhang ZL, Xie YN, Wang L, Yi S, Liu K, Liu J, Pang DW, Zhao XZ (2007) Flow-focusing generation of monodisperse water droplets wrapped by ionic liquid on microfluidic chips: from plug to sphere. Langmuir 23:11924–11931. doi:10.1021/la701170s

Wesseling P (2001) Principles of computational fluid dynamics. Springer, Berlin. doi:10.1007/978-3-642-05146-3

Wong SH, Ward MCL, Wharton CW (2004) Micro T-mixer as a rapid mixing micromixer. Sens Actuators B Chem 100:359–379. doi:10.1016/j.snb.2004.02.008

Xuan X, Zhu J, Church C (2010) Particle focusing in microfluidic devices. Microfluid Nanofluid 9:1–16. doi:10.1007/s10404-010-0602-7

Zhang Z, Zhao P, Xiao G, Lin M, Cao X (2008) Focusing-enhanced mixing in microfluidic channels. Biomicrofluidics 2:1–9. doi:10.1063/1.2894313

Zhou J, Kasper S, Papautsky I (2013) Enhanced size-dependent trapping of particles using microvortices. Microfluid Nanofluid 15:611–623. doi:10.1007/s10404-013-1176-y